Increasing precipitation due to climate change could partially offset the impact of warming air temperatures on glacier loss in the monsoon-influenced Himalaya until 2100 CE

Anya M. Schlich-Davies[1*], Ann V. Rowan[2*], Andrew N. Ross[1], Duncan J. Quincey[3], Vivi K. Pedersen[4]

[1]Priestley International Centre for Climate, School of Earth and Environment, University of Leeds, UK
[2]Department of Earth Science, University of Bergen and Bjerknes Centre for Climate Research, Bergen, Norway
[3]School of Geography, University of Leeds, UK
[4]Department of Geoscience, Aarhus University, Aarhus C, Denmark

*These authors contributed equally to this work
Correspondence to: Ann V. Rowan (ann.rowan@uib.no)

Abstract. Glacier volume in the Himalaya is projected to shrink by 53–70% during this century due to climate change. However, the impact of changes in precipitation amount and distribution on future glacier change remains uncertain because mesoscale meteorology is not represented in current models that project glacier change. We explored the combined effects of past and future changes in air temperature and precipitation amount and distribution on the evolution of Khumbu Glacier in the Everest region of Nepal—a benchmark glacier in the monsoon-influenced Nepal Himalaya—using a climate-glacier modelling approach that forces an ice-dynamical glacier evolution model with a surface mass balance forcing that includes mesoscale meteorological variables derived from downscaling of Regional Climate Model outputs. Our simulations show that historical warming during the late Holocene has committed Khumbu Glacier to future volume loss of 10–23% during this century. Under moderate future warming (RCP4.5) from the present day, Khumbu Glacier could lose 70% volume by 2100 CE due to increasing air temperatures. However, the projected increase in precipitation in tandem with climate warming could offset half of this loss, such that the total decrease in glacier volume by 2100 CE compared to the present day is only 34%. Extreme future warming (RCP8.5) will not be compensated by changes in precipitation but will instead result in substantial ablation above 6,000 m, causing the highest glacier on Earth to vanish between 2160–2260 CE.

1. Introduction

Projecting glacier change in response to climate change is important for determining the impact of anthropogenic warming on regional water availability (Pritchard, 2019). However, such projections remain challenging because accumulation and ablation processes in mountain environments are driven by orographic feedbacks between high-relief topography and atmospheric circulation systems such as the South Asian Summer Monsoon (Bookhagen and Burbank, 2006). Combined, High Mountain Asia is projected to lose 34 ± 19% of glacier volume by 2100 CE if warming is limited to 1.5°C to meet the ambitious Paris Agreement target (Kraaijenbrink et al., 2017) whereas more realistic projections of glacier change give 53 ± 23% volume loss under the moderate warming scenario RCP4.5 and 69 ± 20% under the extreme warming scenario RCP8.5 (Kraaijenbrink et al., 2017; Marzeion et al., 2020; Rounce et al., 2023). However, large uncertainties remain in projections of regional glacier change because of limitations in understanding of the interactions between the mass balance regimes of monsoon-influenced glaciers where accumulation and ablation both occur during the monsoon season and the dynamics of glaciers flowing through high-relief topography (Dehecq et al., 2019; Miles et al., 2018b; Salerno et al., 2023). In the monsoon-influenced Himalaya, changes in the extent and intensity of the Indian Summer Monsoon affected glacier expansion through changes in snowfall during the Last Glacial Maximum (Benn and Owen, 1998; Owen et al., 2009). Future Indian Summer Monsoon precipitation and variability is projected by Global Circulation Models (GCMs) to increase with current global warming (Katzenberger et al., 2021) but the effects of future changes in the monsoon on Himalayan glaciers in terms of precipitation amount, timing, and phase (snow/rain) remain poorly constrained (Immerzeel et al., 2012; Mölg et al., 2014; Ragettli et al., 2016; Shaw et al., 2022; Shea et al., 2015).

Glaciological processes such as the formation and evolution of supraglacial debris, which cover 4–7% of glacier surfaces globally and 30% of the glacier ablation areas in the Himalaya, further modify glacier response to climate change away from the trends predicted from regional mass balance calculations (Herreid and Pellicciotti, 2020; Kraaijenbrink et al., 2017; Rounce et al., 2023; Rowan et al., 2015). While satellite observations show that rates of glacier mass loss across the Himalaya have accelerated over the last 40 years for both clean-ice glaciers and debris-covered glaciers (Maurer et al., 2019), observations and models indicate that thick supraglacial debris has historically reduce mass loss (King et al., 2020; Rounce et al., 2023; Rowan et al., 2021) but this dampening effect is being overturned by the development of supraglacial ponds and ice cliffs within debris layers (Miles et al., 2018a; Strickland et al., 2023). In common with many large Himalayan glaciers that are debris-covered, Khumbu Glacier is in greater imbalance with climate than a climatically equivalent clean-ice glacier, and has maintained a more extensive ice volumes than would be possible without supraglacial debris through the late Holocene (~2 ka). However, recent rapid climate warming has caused extensive mass loss across the entire ablation area, with maximum rates of surface lowering observed in the upper ablation area where the debris layer is thinnest (King et al., 2020). As a result of greater mass loss occurring in the upper ablation area, the lower part of the ablation area is dynamically detached from the active glacier such that ice does not flow from the accumulation area into this section of the glacier (Rowan et al., 2021; Watson et al., 2017). This process of detachment and decay of the former ablation area is extended in time for debris-covered glaciers by the insulation of the ice surface, such that the terminus of the actively flowing glacier remains in contact with the detached ice tongue rather than receding upvalley (Pellicciotti et al., 2015; Quincey et al., 2009; Rowan et al., 2021). The high proportion of debris-covered glaciers in the monsoon-influenced Himalaya means that these processes will significantly affect regional glacier evolution and yet few studies currently consider their impact (Rounce et al., 2023). Projections of glacier evolution in the Himalaya therefore need to account for the feedbacks between debris transport, mass balance, and ice flow (Nicholson et al., 2021) that promote a longer dynamic response compared to climatically equivalent clean-ice glaciers (Rowan et al., 2015).

In this study we target Khumbu Glacier in the Everest region of Nepal, the highest glacier on Earth (flowing from 7,981 m above sea level (a.s.l.) to 4,879 m a.s.l.) and a benchmark debris-covered glacier in the monsoon-influenced Himalaya that is representative of the majority of glaciers in this region (Fig. 1). We used a novel climate-glacier modelling approach to simulate the evolution of Khumbu Glacier from the late Holocene through the present day (2015 CE) until 2100 CE forced by three downscaled Regional Climate Model (RCM) outputs under two Relative Concentration Pathways (RCPs; RCP4.5 and RCP8.5) (Collins et al., 2013) and continued these simulations to 2300 CE using the best available projections of longer-term climate change. The downscaled RCM outputs were used to calculate mass balance time slices using a surface energy balance model, which then forced a dynamic glacier evolution model. Our approach results in a total of six simulations from three RCMs and two RCPs to explore the impacts of possible variability in future precipitation amount and distribution in tandem with climate warming on glacier volume and dynamics. The experimental design represents an advance compared with previous climate-glacier modelling efforts through including robust representations of; (1) mesoscale meteorological phenomena, (2) the processes that redistribute the surface mass balance including snow avalanching and sublimation, and (3) consideration of the feedbacks between supraglacial debris transport, mass balance, and ice flow. The climate-glacier model experimental design used here aims to calculate mesoscale meteorology at an appropriate scale to represent the mass balance of a high-elevation glacier in the monsoon-influenced Himalaya combined with a sophisticated glacier evolution model to represent the processes occurring at the surface that significantly affect glacier mass balance.

2. Models and data

In our climate-glacier modelling approach we use RCMs to force the future climate scenarios. However, to assess the fidelity of these RCMs, we first assess their capabilities against present-day climate and use these results to provide an estimate of the present-day glacier mass balance to force the dynamic glacier model (Fig. 2). We made a total of six numerical experiments, including three downscaled RCMs under two future climate scenarios (RCP4.5 and RCP8.5) and using time slices representing the present day (2015–2020 CE) and the end of the 21st Century (2095–2100 CE). These climate time slices, representing five-year periods, were chosen to reduce the computational expense of the climate-glacier modelling (~24 hours per simulation) and the preceding decade was used for comparison with the climate time slices. Combined, the three RCMs and two future RCPs represent a range of possible future climates including distinctly different precipitation trends. The resulting six climate scenarios were used as inputs to the surface energy balance model COSIPY (Sauter et al. 2020). The resulting six mass balances (present day and future for each RCM) were then used to force the glacier model (Rowan et al., 2015) from the late Holocene through the present day until 2100 CE.

2.1 Present-day RCM downscaling using meteorological observations

RCMs were assessed on their fidelity to present-day climate, also known as hindcasting (Biemans et al., 2013), with emphasis on temperature seasonality and seasonal precipitation dynamics given the importance of these variables for glacier mass balance. RCMs from the Coordinated Regional Downscaling Experiment (CORDEX) South Asia domain dynamically downscaled from CMIP5 GCMs by the Indian Institute of Tropical Meteorology to a 50 km spatial resolution (Lutz et al., 2016) were downloaded for the grid box nearest to Khumbu Glacier (27.9065056°N, 86.4352951°E) at about 2,100 m a.s.l.. Three of the six available CORDEX South Asia RCMs (NOAA, CCCma, IPSL) were selected as discrete scenarios that span the range of possible future precipitation conditions (Table 1); either wet, moderate, or dry climate in 2080–2100 CE. The NOAA RCM is characterised by the highest annual precipitation, the IPSL RCM is characterised by the lowest annual precipitation, and the CCCma RCM is characterised by an intermediate value. The three RCMs span the range of possible future precipitation scenarios and were downscaled using quantile mapping evaluated against observations from high-elevation automatic weather stations (AWS). Indeed, observations from AWS (Fig. 1c) collected between January 2006 and November 2019 were used to aid RCM downscaling with gaps filled with interpolated data from neighbouring stations where possible (Fig. 2). Quantile mapping also known as “distribution mapping”, was used to statistically downscale the daily climate data using 14 years of observations from three AWS. Parametric quantile mapping (Piani et al., 2010) was used whereby a statistical relationship between the raw climate model outputs and observations is formed by substituting the RCM results with observations at a cumulative density function of the prescribed distribution (e.g. a gaussian distribution for temperature; Luo et al., 2018; a gamma distribution for precipitation; Piani et al., 2010). This correction was then applied to the raw RCM outputs to produce a third downscaled dataset to better match observations (Maraun, et al., 2016). The quantile mapping approach is effective for the challenge of downscaling of precipitation and reduces errors in the standard deviation, the coefficient of variation, and the skewness of distributed values relative to other methods (Lafon et al., 2012; Reiter et al., 2018). AWS data were used to disaggregate daily downscaled present-day and end-of-century climate model outputs to the hourly resolution required for the energy balance modelling using seasonal means to reproduce the ‘nocturnal peak’ seen during the monsoon. The MELODIST Python tool was used to disaggregate all other meteorological variables (Förster et al., 2016).

The 14 years of meteorological observations were derived from the two Pyramid AWS at 5,050 m a.s.l and at 5,035 m a.s.l and the West Changri Nup Glacier AWS at 5,363 m a.s.l.. Missing data were replaced through interpolation with an alternative AWS in this group. Precipitation was measured at 15-minute intervals using a Geonor T-200BM sensor mounted 1.8 m above the surface. Evaporation from the bucket is supposedly blocked by a layer of oil but some does occur as evidenced by precipitation values below 0 mm. Noise from wind and evaporation were corrected for by compensating any negative change over the 15-minute time step with the neighbouring positive value such that accumulated precipitation was unchanged. Periods with prolonged evaporation were set to zero. Undercatch of snowfall by rainfall gauges was corrected through precipitation phase partitioning using wind speed observations (Wagnon et al., 2009). For interpolation of air temperature, hourly lapse rates were used that averaged 0.00554 °C m^{-1} to adjust to the height of the reference point at 5,050 m a.s.l.. Where possible, precipitation data taken from the Pyramid AWS at 5,035 m a.s.l. because this precipitation gauge provides a longer period of continuous observations than the other gauges and avoids errors due to low precipitation amounts measured by tipping bucket gauges, which are known to systematically underestimate snowfall, particularly during high winds (Sherpa et al., 2017).

2.2 Future RCM downscaling

Two future RCM climate scenarios (RCP4.5 and RCP8.5) are available from CORDEX South Asia that represent moderate and extreme warming by 2100 CE relative to the present day. These scenarios are frequently used in climate impact studies, enabling comparison with studies that use other climate or glacier model projections. The two future climate scenarios were analysed for each of the three CORDEX RCMs to recognise the inherent high uncertainty on future precipitation trends and the interplay of changing precipitation with atmospheric warming for glacier evolution. The same statistical downscaling approach and disaggregation used for the present day RCMs was applied to the raw CORDEX RCM daily outputs for the future time slices under RCP4.5 and RCP8.5. Downscaled future climates were compared with those found in other studies using CORDEX results and we found similar annual and seasonal temperature trends for the region strongly linked to the choice of RCP, and positive precipitation trends with poor agreement between RCMs (Kaini et al., 2019; Sanjay et al., 2017). The relationship between precipitation and the two future scenarios (RCP4.5 and RCP8.5) was less clear than that for air temperature because the monsoon-influenced Himalaya shows particularly poor RCM consensus and high levels of uncertainty in future precipitation trends with warming relative to other regions in High Mountain Asia (Sanjay et al., 2017). Given the absence of regional climate projections beyond 2100 CE, globally projected temperature changes were used to extend the end-of-century mass balances for RCP4.5 and RCP8.5 . This approach gives rise to a further increase in temperature under RCP4.5 of 0.5 °C by 2200 CE and 0.7 °C by 2300 CE, and a further increase in temperature under RCP8.5 of 2.8 °C by 2200 CE and 4.1 °C by 2300 CE (Collins et al., 2013). For the same reasons, no precipitation changes were applied to the post-2100 CE climates due to the absence of projections for precipitation in the CORDEX RCMs and high uncertainty in global precipitation changes over this period.

2.3 Surface energy and mass balance calculation using COSIPY

The Coupled Snowpack and Ice-surface Energy and Mass Balance model in Python (COSIPY) was used to calculate surface energy balance (Sauter et al., 2020). COSIPY is developed and modularised in Python and integrates a surface energy balance model with a multi-layer snow and ice model and thereby resolves all energy fluxes at the ice surface that contribute to surface melt. COSIPY has previously been applied to glaciers in High Mountain Asia and includes a calculation of sublimation, which is an important ablation process for high-elevation glaciers (Bonekamp et al., 2021; Brun et al., 2023; Huintjes et al., 2015). The COSIPY model domain was taken from the 30-m digital elevation model (DEM) acquired from the Shuttle Radar Topography Mission (Farr et al., 2007) that was resampled to 100-m grid spacing. CORDEX RCM daily climate variables (temperature, precipitation, the radiation components, wind speed, relative humidity and atmospheric pressure) were used to force COSIPY. Snowfall measurements can be used as an input to COSIPY, but precipitation was partitioned into rainfall and snowfall using the snow transfer scheme within COSIPY given the paucity of observations and high uncertainties associated with the AWS observations, climate reanalysis and modelled products for this region (Sauter et al., 2020). COSIPY was forced using hourly meteorology with nine variables to calculate the energy balance and mass balance components at an hourly time step from the sum of accumulation by solid precipitation, deposition, and refreezing of melt water percolation, and ablation by melt and sublimation. The impact of supraglacial debris on ablation rates and avalanching on accumulation rates was handled subsequently in the glacier evolution model.

2.4 Glacier evolution modelling

Here we use the second-order shallow ice approximation model (iSOSIA), a 3-D higher-order ice-dynamical glacier evolution model that solves for the flow of ice including longitudinal and transverse stress gradients that are imposed on ice flow through high-relief topography (Egholm et al., 2011). While previous versions of this model used depth-integrated ice flow, the version used to simulate Khumbu Glacier in this and earlier studies is fully 3-D as the ice thickness is divided into 20 vertical layers to allow for the calculation of englacial ice flow and debris transport (Rowan et al., 2015). The glacier model has a variable time step that can adjust up to a maximum of 0.1 years to allow greater computational efficiency. This glacier model simulates the evolution of debris-covered glaciers by incorporating the feedbacks between debris transport, mass balance and ice flow (Rowan et al., 2015). This glacier model includes two processes that are important for many Himalayan glaciers—the redistribution of snow by avalanching that is estimated to account for 75% of glacier accumulation, and the formation of a supraglacial debris layer that insulate the ice surface and significantly modify ablation (Fig. 1d) (Anderson and Anderson, 2016; Rowan et al., 2015).

The distributed mass balances calculated using COSIPY (forced by the downscaled RCMs) were used as input to the glacier model. Surface processes within the glacier model then modified the distribution of accumulation and ablation. Simulated accumulation was the result of the total snowfall in each cell and avalanching of snow imposed for the accumulated snowpack from hillslopes by removing snow and ice from hillslopes greater than 28° and redistributing this mass across less steep surfaces using a non-linear hillslope flux model (Roering et al., 1999). The avalanching routine was previously applied to Khumbu Glacier and found to be sufficient to prevent snow and ice accumulation on slopes that are observed to be free of glacier ice such as the southwest face of Sagarmatha/Mt. Everest whilst allowing accumulation on steep sections of the glacier (Rowan et al., 2015). The critical slope of 28° was selected because this threshold is low enough to prevent ice accumulation on slopes that are clearly ice-free today, but high enough to produce accumulation rates at the glacier surface that are in line with the limited available observations for Himalayan glaciers of 2 m water equivalent (w.e.) per year (Benn and Lehmkuhl, 2000). Rock avalanching is largely responsible for much of the debris accumulation on the glacier surface, but there is little information about the magnitude and frequency of these events and so headwall erosion was assumed to be uniform at a rate of 1 mm a^{-1} (Rowan et al., 2021). Debris produced by headwall erosion was delivered to the glacier surface using a similar non-linear hillslope flux model to avalanching. The reduction in ablation beneath supraglacial debris from clean-ice values was represented as a reciprocal function that scales clean-ice ablation (b_{clean}) to give sub-debris melt (b_{debris}) as a function of debris thickness (h):

$$b_{debris} = b_{clean} \times \frac{h_0}{h + h_0} \qquad \text{Eq. (1)}$$

where h_0 is a constant representing the characteristic debris thickness at which the reduction in ablation due to insulation by supraglacial debris is 50% of the value for an equivalent clean-ice surface (Anderson and Anderson, 2016; Rowan et al., 2021). The observed heterogeneity of ablation on the surface of Khumbu Glacier requires a parameterisation of sub-debris melt that represents the effects of differential ablation, which is represented in Equation (1) by the value chosen for h_0 (Rowan et al., 2021). The value for h_0 of 0.8 m represents a positively skewed supraglacial debris thickness distribution that includes ablation 'hotspots' such as supraglacial ponds and ice cliffs and is representative of the current state of Khumbu Glacier (Bartlett et al., 2021; Rowan et al., 2021; Strickland et al., 2023).

3. Climate-glacier model experimental design

The late Holocene glacier was reconstructed using a 5000-year equilibrium simulation starting from an ice-free domain. The late Holocene glacier volume was used as the starting point for a transient simulation through the 'Little Ice Age' maximum forced by a step change in mean annual air temperature equivalent to warming of 1.5°C to reach present day conditions. The simulations continued to the present day and 2100 CE forced by the distributed mass balances calculated using COSIPY. For more detail on the glacier model parameterisation, we refer to Rowan et al. (2021).

Khumbu Glacier is surrounded by ice-marginal moraines denoting the late Holocene (1.3 ± 0.1 ka) extent and ice thickness (Hornsey et al., 2022), which are used to constrain the historical spin-up simulation. Observations and modelling of the dynamics and structure of Khumbu Glacier show that the lower 5 km (25% of the total length, 20% of total ice volume) is stagnant and has dynamically detached from the active glacier in the last century (Miles et al., 2021; Quincey et al., 2009; Rowan et al., 2021). Basal ice at the glacier surface indicates that the active terminus overrides the stagnant glacier tongue (Miles et al., 2021) and surface displacement measurements show no longitudinal ice flow through the detached debris-covered tongue, which is instead collapsing laterally at a rate of 3 m a^{-1} (Watson et al., 2017). We therefore simulated only the active section of the glacier and assigned the stagnant mass of the detached debris-covered tongue to the model domain as a static topographic feature. The ice-free domain was found by subtracting estimated ice thickness (Farinotti et al., 2019) from the 30-m DEM. The ice-free model domain incorporated the full hydrological catchment including the steep hillslopes of the Western Cwm that provide snow by avalanching to the glacier surface. The three late Holocene to present-day spin-up simulations of Khumbu Glacier were evaluated against a range of observations at the present day and the simulation forced using the NOAA RCM was identified as the starting point for all future simulations because this was most representative of observed conditions. Greater warming occurred in winter than in summer under both RCPs (Sanjay et al., 2017) and warming air temperatures resulted in an increase in annual precipitation amount of ~15%, with a greater increase in winter precipitation than summer precipitation. As there are no regional temperature projections beyond 2100 CE we used global values to continue the simulations into the next century (Table 1). There are no global projections of precipitation beyond 2100 CE and rather than introduce potentially significant uncertainties into our results by estimating these values, no change in precipitation was applied beyond 2100 CE.

3. Results

3.1 Present-day evaluation of the climate-glacier model results

Each of the downscaled climate variables from the three RCMs for the present-day time slices (2015–2020 CE) were evaluated against 14 years of observations from three AWS to assess the representation of means, seasonality, diurnal cycles, day-to-day variability, and interannual variability. All three downscaled RCMs show good agreement in their mean annual air temperatures (–2.15 ± 0.05°C) and in comparison with observed air temperatures from the Pyramid AWS and the results are presented in Appendix A. The representation of the monsoon was greatly improved by the RCM downscaling: Temperature seasonality was well resolved following quantile mapping and the monthly mean and minimum air temperatures were similar to observations across the present-day time slices (Fig. A1). The monsoon stabilises air temperatures and reduces the range between minimum and maximum temperatures in the downscaled RCMs, which is in better agreement with AWS observations but does not occur in the raw RCMs. We note that the downscaled maximum temperature is at times higher than observations amongst all RCMs during the post-monsoon and winter, however, the distribution of downscaled temperatures shows a good match to observations (Fig. A2). Gamma distribution quantile mapping substantially improved the absolute precipitation values, with the result that the overestimation of winter precipitation and relative underestimation of monsoon precipitation amounts in the raw RCMs was reduced and the downscaled results showed a clearer monsoon signal (Fig. A3). When compared with AWS observations, RCM downscaling slightly over-corrected the seasonal precipitation pattern, with a slight underestimation of winter precipitation for the most extreme winter events. Across the three present-day simulations, the mass balance calculated using the NOAA RCM was more positive than for the ISPL and CCCma RCMs and closer to the mass balance forced by the meteorological observations.

The simulated glacier extents and dynamics were compared with observations of the present-day state and recent (<50 years) change (Fig. 4). The distributed mass balance following integration with the glacier model to include the effects of melt reduction beneath supraglacial debris was more similar to observations than the clean-ice mass balance forcing calculated by COSIPY. The glacier extent was underestimated if supraglacial debris and avalanching of snow were not simulated (Fig. 5). Particularly, the supraglacial debris feedback of the glacier model reproduced the observed reversed mass balance gradient, and gave the highest ablation rates just below the equilibrium line (Benn and Lehmkuhl, 2000). Simulated glacier area was 7.8 km^2—similar to that obtained from structural mapping in 1979 CE (Nakawo, 1986). Radio-echo sounding in 1999 CE obtained ice thickness estimates close to the active terminus of ~160 m (Gades et al., 2000) and simulated ice thickness at the terminus was 130 m. The simulated active terminus thickness was approximately 175 m in 1999 CE, which agrees well with observations of the glacier thinning here by up to 55 m between 1984 and 2018 (King et al., 2020). Simulated surface elevation change in the lower ablation area was –30 m over 20 years to the present day and similar to values derived from satellite observations for 1984–2015 CE (King et al., 2020). Simulated present-day glacier velocities (Fig. 6) reach a maximum of 220 m a^{-1} and agree closely with remote sensing observations (Altena and Kääb, 2020). The simulated present-day velocities that are a better fit to remote sensing observations than previous simulations using an elevation-dependent mass balance forcing (Rowan et al., 2015, 2021) where the maximum simulated velocities were 118 m a^{-1}. Altena and Kääb (2020) estimated velocities of just over 1 m d^{-1} through the Khumbu icefall using satellite image matching compared with mountaineers' navigation devices from May 2018. Feature-tracking estimates of the upper ablation area of Khumbu Glacier indicate velocities of up to 20 m a^{-1} (Quincey et al., 2009; Dehecq et al. 2019). We note that the simulated present-day velocities are a better match to surface displacement observations than previous simulations using an elevation-dependent mass balance forcing (Rowan et al., 2015, 2021).

3.2 Climate change and glacier evolution from the present day until 2100 CE

Khumbu Glacier is responding to historical climate change and would continue to shrink even if warming ceased today. Indeed, if we allow the spin-up experiment to reach equilibrium with the present-day NOAA RCM mass balance, the glacier terminus will recede by 2.1 km and the maximum ice thickness will decrease from 246 m to 206 m by 2100 CE without any additional warming (Fig.7a). In this simulation, a supraglacial debris layer up to 1.3 m thick extended 1 km up-glacier from the terminus and partially dampened the committed loss by sustaining 13% more ice volume than would be the possible for a clean-ice glacier surface under the same mass balance conditions. Therefore the committed glacier volume loss due to historical warming and in the absence of any further climate forcing is 10–23% of the present-day glacier volume (Fig. 7b). Therefore, keeping future warming within the limit of RCP4.5 will limit further shrinking of Khumbu Glacier to only 26% beyond that already committed to by historical climate change.

Considering additional future warming, the climate forcing based on the downscaled NOAA RCM under RCP4.5 was 1.4°C warmer than the present day (–0.75°C in 2095–2100 CE compared with –2.15°C in 2015–2020 CE). For the same climate forcing, the annual precipitation is projected to increase by 14.8% from 581.4 mm at present day to 664.8 mm a^{-1} by 2100 CE, with summer (JJAS) precipitation increasing by 5.4% and winter (DJF) precipitation increasing by 14.1% (Fig. 2). Under RCP8.5, the downscaled NOAA RCM climate forcing is projected to be 3.8°C warmer than present day (1.65°C in 2095–2100 CE) with an annual precipitation increase of 14.9% in 2100 CE, with summer precipitation increasing by 9.8% and winter precipitation increasing by 19.4%. The other RCMs projected greater warming by 2100 CE under RCP4.5, giving warming of 1.6°C (+0.2°C compared with the NOAA RCM) from the present day in the IPSL RCM experiment and 2.2°C (+0.8°C) from the present day in the CCCma RCM experiment. The other RCMs also projected greater warming by 2100 CE under RCP8.5, giving warming of 3.9°C (+0.1°C compared with the NOAA RCM) from the present day for the IPSL RCM experiment and 4.1°C (+0.3°C) from the present day for the CCCma RCM experiment. The projected increase in precipitation amount across the three RCMs was similar between RCPs, giving annual totals above 600 mm by 2100 CE. The moderate CCCma RCM gave the greatest increase in annual precipitation amount of 100 mm by 2100 CE relative to the present day. There was no evidence of change in the intensity of the Indian Summer Monsoon over this period as the seasonal split in precipitation remained similar to the present day, but there was an increase in the frequency of days with high precipitation (>15 mm per day) by 2100 CE, which doubled relative to the present day in the NOAA RCM experiment and was 5–7 times greater relative to the present day in the IPSL RCM experiment.

In the NOAA RCM RCP4.5 experiment, glacier volume decreased by 36% between the present day and 2100 CE (Fig. 7). While significant, the end-of-century glacier loss was partially offset by the concurrent increase in precipitation amount. In comparison, an equivalent simulation forced only by warming and without any change in precipitation resulted in a more linear trajectory of glacier change and 70% loss of glacier volume by 2100 CE (Fig. 8), demonstrating that 34% of potential glacier loss resulting from warming air temperatures could be compensated by the changes in precipitation that will occur as a result of warming air temperatures. The resulting spatially averaged cumulative mass balance was –0.14 m w.e. a^{-1} in 2100 CE, which is slightly more positive than the present-day value of –0.21 m w.e. a^{-1}. Under RCP8.5, all RCM experiments show similar results for mass balance by 2100 CE with only a 10% difference in glacier volume between RCMs (Fig. 7). The CCCma RCM experiment has only a 1% difference in volume loss between RCP4.5 and RCP8.5 by 2100 CE despite a 1.9°C difference in MAAT. This is a surprising result given the significant temperature difference but it can be attributed to the greater number of high-magnitude precipitation events that occur under RCP8.5 in combination with the small difference in winter temperatures between the two RCPs. Indeed, in the CCCma RCM experiment under RCP4.5, maximum winter temperature was 1.7°C higher than for the other RCMs, resulting in ablation and rainfall during the winter.

3.3 Climate change and glacier evolution from 2100 CE until 2300 CE

Projections of climate change beyond 2100 CE are more uncertain than those for this century but do give rise to a clear prognosis for Khumbu Glacier. In all the RCP4.5 experiments, there was little change in glacier volume between 2200 CE and 2300 CE compared to 2100 CE regardless of the RCM forcing used (Table 1 and Fig. 7b). In the NOAA RCP4.5 experiment, the Khumbu Icefall is maintained through to 2300 CE such that ice continues to flow from the Western Cwm to below 6,000 m and the glacier remains in contact with the dynamically detached tongue. Therefore under RCP4.5 Khumbu Glacier could reach a new dynamic equilibrium that maintains a sufficient ice thickness to protect against catastrophic mass loss for at least two centuries. However, substantial glacier loss occurred after 2100 CE in all the RCP8.5 experiments and as a result, Khumbu Glacier completely decayed before 2300 CE. Physical detachment of the debris-covered tongue from the active glacier occurred around 2070 CE in the CCCma and IPSL experiments and around 2140 CE in the NOAA experiment (Fig. 6). We define the glacier to be stagnant at flow at rates less than 10 m a^{-1}, which is a conservative estimate of the uncertainty associated with observations of glacier velocities (Dehecq et al., 2019). Accordingly, we consider Khumbu Glacier to no longer be a viable glacier system at the point where there is no ice flow above this value in the entire glacier since there is minimal throughput of mass through the ice volume. In the NOAA RCP8.5 experiment, the glacier area was 1.2 km^2 and the mean velocity reduced to 10 m a^{-1} by 2260 CE, such that the glacier was no longer viable as an active system. Glacier breakdown occurred earlier for the CCCma and IPSL RCMs because loss of ice volume due to warming was not compensated to the same magnitude by an increase in precipitation as that projected under RCP8.5 using the NOAA RCM.

4. Discussion

4.1 Uncertainties associated with the climate-glacier modelling approach

The climate-mass balance forcing ensemble was limited in size due to the small number of different RCMs available for the CORDEX South Asia region, and we considered all the relevant available forcings. A single RCM was not considered sufficient to represent both present-day climate and potential future climatic extremes. The use of three RCMs allows the implications of uncertainties in understanding of local climate for glacier evolution to be simulated. A multi-model mean approach using all the CORDEX South Asia RCMs, which is widely used elsewhere, was not considered sufficient to represent present-day and future climate conditions in the Khumbu Valley as this approach gives equal weighting to models with poor and good performance in reproducing climate (Pierce et al., 2009). The differences in simulated glacier change and response time that result from the RCM forcings are at times greater than those resulting from the different future RCPs due to differences in projections of precipitation. As the CORDEX CMIP5 and CMIP6 projects only produced dynamically downscaled RCMs for the future climate scenarios RCP4.5 and RCP8.5, the implications of other RCPs for glacier evolution cannot yet be assessed in our study. The representation of the distribution and rates of accumulation were improved following integration of the RCM-forced mass balances with the glacier model adopted here because of the redistribution of snowfall by avalanching mainly from steep hillslopes onto the glacier improves agreement between simulated accumulation rates and expected values for Himalayan glaciers (Benn and Lehmkuhl, 2000). Future work to resolve the impact of low frequency–high magnitude avalanche events on accumulation rates would help to refine this calculation but the contribution of avalanches to glacier accumulation over decadal time scales remains challenging to measure.

Five-year downscaled RCM time slices were chosen to reduce computational expense associated with COSIPY and the integration with the glacier model. To ensure the selected five years were representative of the climate for that period, the preceding decade was also used for comparison with the time slice climate results, although the quantile mapping downscaling method using 14 years of reference AWS data should limit the influence of any natural variability (i.e., by ensuring that the period is not reflecting an extreme phase of natural climate oscillation). This comparison was particularly important for the future time slices where large uncertainties arise between RCMs and there are no observations for evaluation of the downscaled climate or mass balance. An experiment was conducted using mid-century (2045–2050 CE) mass balance forcings to investigate the effect on glacier-climate imbalance. However this experiment produced identical results in 2100 CE to the experiments with no mid-century forcing because the response time of the simulated glaciers was longer than the 40-year period between the present-day and future time slices and so the mid-century mass balance forcing was not considered necessary.

The uncertainties associated with GCM projections increase with time after 2100 CE, particularly under RCP8.5. For example, forecasts of global climate warming for 2281–2300 CE relative to 1986–2005 CE under RCP8.5 range from 3.0°C to 12.6°C (Collins et al., 2013). In the absence of RCMs that can project changes in precipitation after 2100 CE, precipitation was maintained at the same level for the climate-glacier model simulations beyond 2100 CE. The end-of-century precipitation amount is unlikely to be reflective of the more distant future and therefore more realistic precipitation projections are required to explore whether the active glacier can be sustained further into the future or will lose mass more quickly than is found here. However, while such future precipitation changes may be of importance under the RCP4.5 future climate scenario, we do not expect that there will be a sufficient increase in precipitation beyond 2100 CE that could compensate for the projected warming under RCP8.5. The projected temperature changes used to simulate glacier evolution after 2100 CE are global averages and do not include the effects of elevation-dependent warming. Warming is likely to be higher than the global mean for the Khumbu region given that warming over land is generally at least 0.2°C higher than the global mean value (Collins et al., 2013).

4.2 Comparison of outcomes under RCP4.5 and RCP8.5

Current global greenhouse gas emissions are following the trajectory of the moderate warming scenario RCP4.5, and the extreme warming scenario RCP8.5 could be described as ‘low possibility but high impact’ (Pedersen et al., 2020). However, mountain regions are warming more rapidly than the global mean such that a global temperature rise of 1.5°C will lead to 2.1 ± 0.1°C of warming in High Mountain Asia (Kraaijenbrink et al., 2017; Pepin et al., 2022) although the occurrence of elevation-dependent warming above 5,000 m a.s.l. is debated (Gao et al., 2018), and this may suggest that the present long-term projections of glacier volume loss are conservative in nature. High-magnitude precipitation events from winter Westerly disturbances increased by a factor of seven between the present day and 2100 CE in the IPSL RCM under RCP8.5 future climate scenario and could result in net annual glacier mass balances that are less negative than would be the case when solely forced by change in MAAT. However, we found no evidence of future increases in precipitation offsetting RCP8.5 warming—net glacier mass balance was strongly negative in all RCP8.5 experiments and insufficient to maintain an actively flowing glacier. Under RCP8.5, glacier mass balance in the monsoon-influenced Himalaya may therefore shift from being driven by accumulation during the monsoon to predominantly during winter, with monsoon precipitation only resulting in snow accumulation at the very highest elevations being insufficient to maintain flowing glaciers. This outcome is avoidable by limiting anthropogenic warming to within RCP4.5, which, due to the associated increase in precipitation, could sustain nearly two thirds of the current glacier volume until 2100 CE and potentially two centuries further into the future.

Comparing our results to those for the same glacier from a global modelling study forced by an ensemble of 10 GCMs (Rounce et al., 2023) shows that our experiments project less severe rates of ice volume decline resulting in a smaller amount of loss by 2100 CE (Fig. 8). In our experiments, there is 39% less loss under the RCP4.5 future climate scenario and 32% less under RCP8.5 than in the global study. One difference between these results is that rather than using the global glacier inventory outline to define the glacier margins we consider only the actively flowing glacier and so exclude 20% of the starting glacier volume in the detached tongue. We would expect the two sections of the glacier to evolve along different paths: while the active glacier responds to climate change as projected in our experiments, thick supraglacial debris mantling the detached tongue could allow this ice mass to survive and slowly decay *in situ* for many decades beyond the present day. The decay of the detached tongue may however increase due to erosion of the surface by ice cliffs and supraglacial water bodies that are expanding across the former glacier surface.

4.3 Impacts of microscale meteorology on glacier change

While we have considered the effects of mesoscale meteorology on glacier mass balance, smaller-scale processes operating close to the land surface could also be important. Katabatic winds are suggested to explain a local 15-year decrease in maximum air temperatures and precipitation over glaciers while minimum air temperatures continue to rise (Salerno et al., 2023). However, the impact of micro-scale near-surface cooling on the duration and extent of mesoscale precipitation and accumulation is likely to be minimal, and therefore unlikely to significantly affect glacier-wide mass balance (Mott et al., 2020; Shaw et al., 2024). Observations from an AWS on Khumbu Glacier (6,464 m a.s.l.) indicate that surface energy fluxes may be sufficient to cause non-negligible melting of glacier surfaces despite freezing air temperatures (Matthews et al., 2020). Results from an ice core from South Col Glacier (>8,000 m a.s.l.) combined with COSIPY experiments suggested that ablation may also take place at even at the highest elevations (Potocki et al., 2022). However, a subsequent study of the same glacier found no evidence of change, and identified large uncertainties associated with simulating mass balance at these extreme elevations where sub-daily air temperature gradients and the duration of snow cover strongly affect ablation and accumulation (Brun et al., 2023). Our results show that avalanching and sublimation are important controls on recent and future glacier evolution for Khumbu Glacier. Our study addresses these finer-scale temporal (hourly) and spatial (100 m) processes that affect glacier mass balance across the elevation range of Khumbu Glacier, but further observations of meteorological and glaciological conditions at the highest elevations would be beneficial, and needed if micro-scale processes were to be included in future glacier modelling efforts (Brun et al., 2023; Khadka et al., 2021; Mölg et al., 2014; Shaw et al., 2022).

4.4 The response of large debris-covered glaciers to climate change

The dynamic response time of large glaciers to climate change is of the order of centuries, and significant changes in glacier volume continue after an imposed forcing ceases. For this reason, we start our simulations from the late Holocene (around 1.3 ka) when Khumbu Glacier was last considered dynamically stable (Hornsey et al., 2022; Rowan et al., 2015). The relationship between response time and mass balance becomes less important after 2100 CE when the glacier is so small that any dynamic behaviour has little impact on volume change. Global and regional glacier modelling studies typically start their simulations in the current century (e.g., 2000–2007 CE (Marzeion et al., 2020); 2015 CE (Rounce et al., 2023) and a further complication arises from the use of global glacier inventories as a starting point for glacier modelling studies, as such inventories cannot capture the current dynamic state of glaciers that are imbalanced and so include all ice-covered areas rather than identifying actively flowing ice. However, satellite-derived velocity products do identify where ice flow within glacier outlines declines to negligible rates (Dehecq et al., 2019). The RGI 7.0 inventory for Khumbu Glacier is based on imagery from 1999 CE (RGI 7.0 Consortium, 2023) where the detached debris-covered tongue represents 20% of the glacier volume contained within this outline (Fig. 1c). Simulations that integrated the stagnant tongue into the model domain rather than as part of the flowing ice improved the representation of simulated ice flow compared to observed values, supporting our conclusion that the debris-covered tongue has been dynamically detached from the active glacier for 50–100 years (Rowan et al., 2021). Additionally, field observations support the active and stagnant sections co-existing in contact with each other, as englacial optical televiewing indicates that thrusting occurs at several sites denoted by skewed internal debris layers and of basal ice that has been thrust to the glacier surface near to the Changri Nup palaeoconfluence from the direction of Khumbu icefall (Miles et al., 2021). Our simulations show that development of supraglacial debris at the terminus reduces net loss (Fig. 5) but otherwise the glacier surface is clean (Fig. 4). Therefore, while supraglacial debris sustains about 13% of additional glacier volume compared to a clean-ice surface, the local mass balance gradient is a more important control on glacier change for both clean-ice glaciers and debris-covered Himalayan glaciers.

5. Conclusions

In the monsoon-influenced Himalaya, 85% of glacier area is located above 5,000 m and 21% is above 6000 m. Despite these high elevations, Himalayan glaciers are rapidly losing ice volume in response to climate change. Himalayan glaciers are projected to shrink by 53% to 70% during this century due to global climate change. However, the impact of future precipitation change on glacier change remains uncertain because mesoscale meteorology is not often represented in glacier modelling studies. We explore the effects of future changes in air temperature and precipitation by simulating the evolution of Khumbu Glacier in the Everest region of Nepal—a benchmark glacier in the monsoon-influenced Nepal Himalaya—using mesoscale climate-glacier modelling. Historical warming commits Khumbu Glacier to future volume loss of 10–23% by 2100 CE. We show that while moderate future warming (equivalent to future climate scenario RCP4.5) will lead to glacier volume loss of 70% by 2100 CE, the projected concurrent increase in precipitation amount will offset 34% of this change and reduce the glacier loss by about a half. However, extreme future warming (RCP8.5) will not be compensated by changes in precipitation amount, but will instead result in substantial ablation above 6,000 m and cause the highest glacier on Earth to vanish by 2160–2260 CE. Our results project the mass balance of Khumbu Glacier under RCP4.5 as close to zero in 2100 CE, with slightly differing ice volumes remaining between experiments depending on the Regional Climate Model forcing used. Therefore, if climate change is limited to the moderate end-of-century scenario RCP4.5, Khumbu Glacier will lose about a third of its volume and the active terminus will recede to the base of the icefall with insignificant further change in glacier volume beyond this point in time. In this scenario, Khumbu Glacier has a similar extent in 2100 CE to the active section of the present-day glacier and is at least one example of how monsoon-influenced Himalayan glaciers could persist into the future if global efforts are sufficient to mitigate anthropogenic climate change.

Code availability

The COSIPY surface energy balance model is available from the original publication describing this model (Sauter et al., 2020). The version of the glacier model used in this study is available from Zenodo (Rowan, 2024).

Data availability

Daily data from the Coordinated Regional Downscaling Experiment (CORDEX) South Asia domain were downloaded from the Indian Institute of Tropical Meteorology website (http://cccr.tropmet.res.in/home/cordexsa_about.jsp) for the grid box nearest to Khumbu Glacier (27.9065°N, 86.4353°E). Incoming shortwave and longwave radiation components were downloaded from the ESGF portal (https://esgf-ui.ceda.ac.uk/cog/projects/cordex-ceda/). 14 years of meteorological observations were derived from the two Pyramid AWS at 5,050 m a.s.l and at 5,035 m a.s.l (SHARE network Ev-K2-CNR; https://www.evk2cnr.org) and the West Changri Nup glacier AWS at 5,363 m a.s.l (GlacioClim: https://glacioclim.osug.fr/).

Author contributions

Conceptualisation: DJQ, ANR, AVR
Data curation: ASD, ANR, AVR
Formal analysis: ASD, ANR, AVR
Funding acquisition: DJR, ANR
Investigation: ASD
Methodology: ASD, ANR, AVR, VKP
Project administration: DJQ, ANR
Resources: DJQ, ANR
Software: AVR, VKP
Supervision: DJQ, ANR, AVR
Validation: ASD, AVR
Visualisation: ASD, AVR
Writing – original draft preparation: ASD, AVR, DJQ, ANR, VKP
Writing – review and editing: ASD, AVR, DJQ, ANR, VKP

Competing interests

The authors declare that they have no conflict of interest.

Acknowledgements

Tobias Sauter and Anselm Arndt are thanked for support in using COSIPY. We thank Patrick Wagnon for sharing the Pyramid and Changri Nup Glacier automatic weather station data. We thank David Rounce for sharing global glacier model results for Khumbu Glacier from Rounce et al. (2023). Some of the simulations presented were performed on resources provided by Sigma2, the National Infrastructure for High-Performance Computing and Data Storage in Norway.

Financial support

ASD was supported by the Priestley International Centre for Climate at the University of Leeds, and a University of Leeds Anniversary Research Scholarship. AVR was supported by a Royal Society Dorothy Hodgkin Research Fellowship (DHF\R1\201113).

References

Altena, B. and Kääb, A.: Ensemble matching of repeat satellite images applied to measure fast-changing ice flow, verified with mountain climber trajectories on Khumbu icefall, Mount Everest, J. Glaciol., 66, 905–915, https://doi.org/10.1017/jog.2020.66, 2020.

Anderson, L. S. and Anderson, R. S.: Modeling debris-covered glaciers: response to steady debris deposition, The Cryosphere, 10, 1105–1124, https://doi.org/10.5194/tc-10-1105-2016, 2016.

Bartlett, O. T., Ng, F. S. L., and Rowan, A. V.: Morphology and evolution of supraglacial hummocks on debris-covered Himalayan glaciers, Earth Surf. Process. Landforms, 46, 525–539, https://doi.org/10.1002/esp.5043, 2021.

Benn, D. I. and Lehmkuhl, F.: Mass balance and equilibrium-line altitudes of glaciers in high-mountain environments, Quaternary International, 65–66, 15–29, https://doi.org/10.1016/S1040-6182(99)00034-8, 2000.

Benn, D. I. and Owen, L. A.: The role of the Indian summer monsoon and the mid-latitude westerlies in Himalayan glaciation: review and speculative discussion, Journal of the Geological Society, 155, 353–363, https://doi.org/10.1144/gsjgs.155.2.0353, 1998.

Bonekamp, P. N. J., Wanders, N., Wiel, K., Lutz, A. F., and Immerzeel, W. W.: Using large ensemble modelling to derive future changes in mountain specific climate indicators in a 2 and 3°C warmer world in High Mountain Asia, Int J Climatol, 41, https://doi.org/10.1002/joc.6742, 2021.

Bookhagen, B. and Burbank, D. W.: Topography, relief, and TRMM-derived rainfall variations along the Himalaya, Geophys. Res. Lett., 33, L08405, https://doi.org/10.1029/2006GL026037, 2006.

Brun, F., King, O., Réveillet, M., Amory, C., Planchot, A., Berthier, E., Dehecq, A., Bolch, T., Fourteau, K., Brondex, J., Dumont, M., Mayer, C., Leinss, S., Hugonnet, R., and Wagnon, P.: Everest South Col Glacier did not thin during the period 1984–2017, The Cryosphere, 17, 3251–3268, https://doi.org/10.5194/tc-17-3251-2023, 2023.

Collins, M., Knutti, R., and Arblaster, J.: Long-term Climate Change: Projections, Commitments and Irreversibility. In: Climate Change 2013: The Physical Science Basis. Contribution of Working Group I to the Fifth Assessment Report of the Intergovernmental Panel on Climate Change [Stocker, T.F., D. Qin, G.-K. Plattner, M. Tignor, S.K. Allen, J. Boschung, A. Nauels, Y. Xia, V. Bex and P.M. Midgley (eds.)]. Cambridge University Press, Cambridge, United Kingdom and New York, NY, USA,, 1–108., 2013.

Debele, B., Srinivasan, R., and Yves Parlange, J.: Accuracy evaluation of weather data generation and disaggregation methods at finer timescales, Advances in Water Resources, 30, 1286–1300, https://doi.org/10.1016/j.advwatres.2006.11.009, 2007.

Dehecq, A., Gourmelen, N., Gardner, A. S., Brun, F., Goldberg, D., Nienow, P. W., Berthier, E., Vincent, C., Wagnon, P., and Trouvé, E.: Twenty-first century glacier slowdown driven by mass loss in High Mountain Asia, Nature Geosci, 12, 22–27, https://doi.org/10.1038/s41561-018-0271-9, 2019.

Egholm, D. L., Knudsen, M. F., Clark, C. D., and Lesemann, J. E.: Modeling the flow of glaciers in steep terrains: The integrated second-order shallow ice approximation (iSOSIA), J. Geophys. Res., 116, https://doi.org/10.1029/2010JF001900, 2011.

Farinotti, D., Huss, M., Fürst, J. J., Landmann, J., Machguth, H., Maussion, F., and Pandit, A.: A consensus estimate for the ice thickness distribution of all glaciers on Earth, Nat. Geosci., 12, 168–173, https://doi.org/10.1038/s41561-019-0300-3, 2019.

Farr, T. G., Rosen, P. A., Caro, E., Crippen, R., Duren, R., Hensley, S., Kobrick, M., Paller, M., Rodriguez, E., Roth, L., Seal, D., Shaffer, S., Shimada, J., Umland, J., Werner, M., Oskin, M., Burbank, D., and Alsdorf, D.: The Shuttle Radar Topography Mission, Reviews of Geophysics, 45, 2005RG000183, https://doi.org/10.1029/2005RG000183, 2007.

Förster, K., Hanzer, F., Winter, B., Marke, T., and Strasser, U.: An open-source MEteoroLOgical observation time series DISaggregation Tool (MELODIST v0.1.1), Geosci. Model Dev., 9, 2315–2333, https://doi.org/10.5194/gmd-9-2315-2016, 2016.

Gades, A., Conway, H., Nereson, N., Naito, N., and Kadota, T.: Radio echo-sounding through supraglacial debris on Lirung and Khumbu Glaciers, Nepal Himalayas, Debris-Covered Glaciers (Proceedings of a workshop held at Seattle, Washington, USA, September 2000). IAHS, 264, 13–22, 2000.

Gao, Y., Chen, F., Lettenmaier, D. P., Xu, J., Xiao, L., and Li, X.: Does elevation-dependent warming hold true above 5000 m elevation? Lessons from the Tibetan Plateau, npj Clim Atmos Sci, 1, 19, https://doi.org/10.1038/s41612-018-0030-z, 2018.

Herreid, S. and Pellicciotti, F.: The state of rock debris covering Earth’s glaciers, Nat. Geosci., 13, 621–627, https://doi.org/10.1038/s41561-020-0615-0, 2020.

Hornsey, J., Rowan, A. V., Kirkbride, M. P., Livingstone, S. J., Fabel, D., Rodes, A., Quincey, D. J., Hubbard, B., and Jomelli, V.: Be-10 Dating of Ice-Marginal Moraines in the Khumbu Valley, Nepal, Central Himalaya, Reveals the Response of Monsoon-Influenced Glaciers to Holocene Climate Change, JGR Earth Surface, 127, https://doi.org/10.1029/2022JF006645, 2022.

Huintjes, E., Neckel, N., Hochschild, V., and Schneider, C.: Surface energy and mass balance at Purogangri ice cap, central Tibetan Plateau, 2001–2011, J. Glaciol., 61, 1048–1060, https://doi.org/10.3189/2015JoG15J056, 2015.

Immerzeel, W. W., van Beek, L. P. H., Konz, M., Shrestha, A. B., and Bierkens, M. F. P.: Hydrological response to climate change in a glacierized catchment in the Himalayas, Climatic Change, 110, 721–736, https://doi.org/10.1007/s10584-011-0143-4, 2012.

Kaini, S., Nepal, S., Pradhananga, S., Gardner, T. and Sharma, A. K. 2019. Representative general circulation models selection and downscaling of climate data for the transboundary Koshi river basin in China and Nepal. International Journal of Climatology 40(9): 4131-4149. doi: 10.1002/joc.6447.

Katzenberger, A., Schewe, J., Pongratz, J., and Levermann, A.: Robust increase of Indian monsoon rainfall and its variability under future warming in CMIP6 models, Earth Syst. Dynam., 12, 367–386, https://doi.org/10.5194/esd-12-367-2021, 2021.

Khadka, A., Matthews, T., Perry, L. B., Koch, I., Wagnon, P., Shrestha, D., Sherpa, T. C., Aryal, D., Tait, A., Sherpa, T. G., Tuladhar, S., Baidya, S. K., Elvin, S., Elmore, A. C., Gajurel, A., and Mayewski, P. A.: Weather on MOUNT EVEREST during the 2019 summer MONSOON, Weather, 76, 205–207, https://doi.org/10.1002/wea.3931, 2021.

King, O., Bhattacharya, A., Ghuffar, S., Tait, A., Guilford, S., Elmore, A. C., and Bolch, T.: Six Decades of Glacier Mass Changes around Mt. Everest Are Revealed by Historical and Contemporary Images, One Earth, 3, 608–620, https://doi.org/10.1016/j.oneear.2020.10.019, 2020.

Kraaijenbrink, P. D. A., Bierkens, M. F. P., Lutz, A. F., and Immerzeel, W. W.: Impact of a global temperature rise of 1.5 degrees Celsius on Asia's glaciers, Nature, 549, 257–260, https://doi.org/10.1038/nature23878, 2017.

Lafon, T. et al. 2012. Bias correction of daily precipitation simulated by a regional climate model: A comparison of methods, International Journal of Climatology 33(6): 1367–1381. doi:10.1002/joc.3518.

Luo, M. et al. (2018). Comparing bias correction methods used in downscaling precipitation and temperature from regional climate models: A case study from the Kaidu River basin in western China. Water 10(8): 1046. doi:10.3390/w10081046.

Lutz, A., Maat, H., Biemans, H., Shrestha, A., Wester, P. and Immerzeel, W., (2016). Selecting representative climate models for climate change impact studies: an advanced envelope-based selection approach. International Journal of Climatology 36(12): 3988-4005.

Maraun D, Wetterhall F, Ireson AM, Chandler RE. Kendon EJ, Widmann M. Brienen S. Rust H. W. Sauter T. Themeßl M. Venema V. K. C. 2010 Precipitation downscaling under climate change: recent developments to bridge the gap between dynamical models and the end user. Reviews of Geophysics 48 (3), RG3003.

Marzeion, B., Hock, R., Anderson, B., Bliss, A., Champollion, N., Fujita, K., Huss, M., Immerzeel, W. W., Kraaijenbrink, P., Malles, J., Maussion, F., Radić, V., Rounce, D. R., Sakai, A., Shannon, S., Van De Wal, R., and Zekollari, H.: Partitioning the Uncertainty of Ensemble Projections of Global Glacier Mass Change, Earth's Future, 8, e2019EF001470, https://doi.org/10.1029/2019EF001470, 2020.

Matthews, T., Perry, L. B., Koch, I., Aryal, D., Khadka, A., Shrestha, D., Abernathy, K., Elmore, A. C., Seimon, A., Tait, A., Elvin, S., Tuladhar, S., Baidya, S. K., Potocki, M., Birkel, S. D., Kang, S., Sherpa, T. C., Gajurel, A., and Mayewski, P. A.: Going to Extremes: Installing the World's Highest Weather Stations on Mount Everest, Bulletin of the American Meteorological Society, 101, E1870–E1890, https://doi.org/10.1175/BAMS-D-19-0198.1, 2020.

Maurer, J. M., Schaefer, J. M., Rupper, S., and Corley, A.: Acceleration of ice loss across the Himalayas over the past 40 years, Sci. Adv., 5, eaav7266, https://doi.org/10.1126/sciadv.aav7266, 2019.

Miles, E. S., Willis, I., Buri, P., Steiner, J. F., Arnold, N. S., and Pellicciotti, F.: Surface Pond Energy Absorption Across Four Himalayan Glaciers Accounts for 1/8 of Total Catchment Ice Loss, Geophys. Res. Lett., 45, https://doi.org/10.1029/2018GL079678, 2018a.

Miles, K. E., Hubbard, B., Quincey, D. J., Miles, E. S., Sherpa, T. C., Rowan, A. V., and Doyle, S. H.: Polythermal structure of a Himalayan debris-covered glacier revealed by borehole thermometry, Sci Rep, 8, 16825, https://doi.org/10.1038/s41598-018-34327-5, 2018b.

Miles, K. E., Hubbard, B., Miles, E. S., Quincey, D. J., Rowan, A. V., Kirkbride, M., and Hornsey, J.: Continuous borehole optical televiewing reveals variable englacial debris concentrations at Khumbu Glacier, Nepal, Commun Earth Environ, 2, 12, https://doi.org/10.1038/s43247-020-00070-x, 2021.

Mölg, T., Maussion, F., and Scherer, D.: Mid-latitude westerlies as a driver of glacier variability in monsoonal High Asia, Nature Clim Change, 4, 68–73, https://doi.org/10.1038/nclimate2055, 2014.

Mott, R., Stiperski, I., and Nicholson, L.: Spatio-temporal flow variations driving heat exchange processes at a mountain glacier, The Cryosphere, 14, 4699–4718, https://doi.org/10.5194/tc-14-4699-2020, 2020.

Nakawo, M., Iwata, S., Watanabe, O. and Yoshida, M.: Processes which distribute supraglacial debris on the Khumbu Glacier, Nepal Himalaya. Annals of Glaciology, 8, pp.129-131, https://doi.org/10.3189/S0260305500001294, 1986.

Nicholson, L., Wirbel, A., Mayer, C., and Lambrecht, A.: The Challenge of Non-Stationary Feedbacks in Modeling the Response of Debris-Covered Glaciers to Climate Forcing, Front. Earth Sci., 9, 662695, https://doi.org/10.3389/feart.2021.662695, 2021.

Owen, L. A., Robinson, R., Benn, D. I., Finkel, R. C., Davis, N. K., Yi, C., Putkonen, J., Li, D., and Murray, A. S.: Quaternary glaciation of Mount Everest, Quaternary Science Reviews, 28, 1412–1433, https://doi.org/10.1016/j.quascirev.2009.02.010, 2009.

Pedersen, J. S. T., Van Vuuren, D. P., Aparício, B. A., Swart, R., Gupta, J., and Santos, F. D.: Variability in historical emissions trends suggests a need for a wide range of global scenarios and regional analyses, Commun Earth Environ, 1, 41, https://doi.org/10.1038/s43247-020-00045-y, 2020.

Pellicciotti, F., Stephan, C., Miles, E., Herreid, S., Immerzeel, W. W., and Bolch, T.: Mass-balance changes of the debris-covered glaciers in the Langtang Himal, Nepal, from 1974 to 1999, J. Glaciol., 61, 373–386, https://doi.org/10.3189/2015JoG13J237, 2015.

Pepin, N. C., Arnone, E., Gobiet, A., Haslinger, K., Kotlarski, S., Notarnicola, C., Palazzi, E., Seibert, P., Serafin, S., Schöner, W., Terzago, S., Thornton, J. M., Vuille, M., and Adler, C.: Climate Changes and Their Elevational Patterns in the Mountains of the World, Reviews of Geophysics, 60, https://doi.org/10.1029/2020RG000730, 2022.

Piani, C. et al. 2010. Statistical Bias Correction of global simulated daily precipitation and temperature for the application of Hydrological Models. Journal of Hydrology 395(3–4): 199–215. doi:10.1016/j.jhydrol.2010.10.024.

Pierce, D. W., Barnett, T. P., Santer, B. D., and Gleckler, P. J.: Selecting global climate models for regional climate change studies, Proc. Natl. Acad. Sci. U.S.A., 106, 8441–8446, https://doi.org/10.1073/pnas.0900094106, 2009.

Potocki, M., Mayewski, P. A., Matthews, T., Perry, L. B., Schwikowski, M., Tait, A. M., Korotkikh, E., Clifford, H., Kang, S., Sherpa, T. C., Singh, P. K., Koch, I., and Birkel, S.: Mt. Everest's highest glacier is a sentinel for accelerating ice loss, npj Clim Atmos Sci, 5, 7, https://doi.org/10.1038/s41612-022-00230-0, 2022.

Pritchard, H. D.: Asia's shrinking glaciers protect large populations from drought stress, Nature, 569, 649–654, https://doi.org/10.1038/s41586-019-1240-1, 2019.

Quincey, D. J., Luckman, A., and Benn, D.: Quantification of Everest region glacier velocities between 1992 and 2002, using satellite radar interferometry and feature tracking, J. Glaciol., 55, 596–606, https://doi.org/10.3189/002214309789470987, 2009.

Ragettli, S., Immerzeel, W. W., and Pellicciotti, F.: Contrasting climate change impact on river flows from high-altitude catchments in the Himalayan and Andes Mountains, Proc Natl Acad Sci USA, 113, 9222–9227, https://doi.org/10.1073/pnas.1606526113, 2016.

Reiter, P., Gutjahr, O., Schefczyk, L., Heinemann, G. and Casper, M. 2017. Does applying quantile mapping to subsamples improve the bias correction of daily precipitation? International Journal of Climatology 38(4): 1623–1633. doi:10.1002/joc.5283.

RGI 7.0 Consortium: A Dataset of Global Glacier Outlines, Version 7.0. Boulder, Colorado USA. NSIDC: National Snow and Ice Data Center, https://doi.org/10.5067/f6jmovy5navz, 2023.

Roering, J. J., Kirchner, J. W., and Dietrich, W. E.: Evidence for nonlinear, diffusive sediment transport on hillslopes and implications for landscape morphology, Water Resources Research, 35, 853–870, https://doi.org/10.1029/1998WR900090, 1999.

Rounce, D. R., Hock, R., Maussion, F., Hugonnet, R., Kochtitzky, W., Huss, M., Berthier, E., Brinkerhoff, D., Compagno, L., Copland, L., Farinotti, D., Menounos, B., and McNabb, R. W.: Global glacier change in the 21st century: Every increase in temperature matters, Science, 379, 78–83, https://doi.org/10.1126/science.abo1324, 2023.

Rowan, A. V., Egholm, D. L., Quincey, D. J., and Glasser, N. F.: Modelling the feedbacks between mass balance, ice flow and debris transport to predict the response to climate change of debris-covered glaciers in the Himalaya, Earth and Planetary Science Letters, 430, 427–438, https://doi.org/10.1016/j.epsl.2015.09.004, 2015.

Rowan, A. V., Egholm, D. L., Quincey, D. J., Hubbard, B., King, O., Miles, E. S., Miles, K. E., and Hornsey, J.: The Role of Differential Ablation and Dynamic Detachment in Driving Accelerating Mass Loss From a Debris-Covered Himalayan Glacier, J. Geophys. Res. Earth Surf., 126, https://doi.org/10.1029/2020JF005761, 2021.

Rowan, A.V., annvrowan/isosia: iSOSIA version used in Schlich-Davies et al. (spm-3.3.3r). Zenodo. https://doi.org/10.5281/zenodo.12666864, 2024

Salerno, F., Guyennon, N., Yang, K., Shaw, T. E., Lin, C., Colombo, N., Romano, E., Gruber, S., Bolch, T., Alessandri, A., Cristofanelli, P., Putero, D., Diolaiuti, G., Tartari, G., Verza, G., Thakuri, S., Balsamo, G., Miles, E. S., and Pellicciotti, F.: Local cooling and drying induced by Himalayan glaciers under global warming, Nat. Geosci., 16, 1120–1127, https://doi.org/10.1038/s41561-023-01331-y, 2023.

Sanjay, J., Krishnan, R., Shrestha, A. B., Rajbhandari, R., and Ren, G.-Y.: Downscaled climate change projections for the Hindu Kush Himalayan region using CORDEX South Asia regional climate models, Advances in Climate Change Research, 8, 185–198, https://doi.org/10.1016/j.accre.2017.08.003, 2017.

Sauter, T., Arndt, A., and Schneider, C.: COSIPY v1.3 – an open-source coupled snowpack and ice surface energy and mass balance model, Geosci. Model Dev., 13, 5645–5662, https://doi.org/10.5194/gmd-13-5645-2020, 2020.

Shaw, T. E., Miles, E. S., Chen, D., Jouberton, A., Kneib, M., Fugger, S., Ou, T., Lai, H.-W., Fujita, K., Yang, W., Fatichi, S., and Pellicciotti, F.: Multi-decadal monsoon characteristics and glacier response in High Mountain Asia, Environ. Res. Lett., 17, 104001, https://doi.org/10.1088/1748-9326/ac9008, 2022.

Shaw, T. E., Buri, P., McCarthy, M., Miles, E. S., and Pellicciotti, F.: Local Controls on Near-Surface Glacier Cooling Under Warm Atmospheric Conditions, JGR Atmospheres, 129, e2023JD040214, https://doi.org/10.1029/2023JD040214, 2024.

Shea, J. M., Immerzeel, W. W., Wagnon, P., Vincent, C., and Bajracharya, S.: Modelling glacier change in the Everest region, Nepal Himalaya, The Cryosphere, 9, 1105–1128, https://doi.org/10.5194/tc-9-1105-2015, 2015.

Sherpa SF, Wagnon P, Brun F, Berthier E, Vincent C, Lejeune Y, Arnaud Y, Kayastha RB, Sinisalo A. 2017. Contrasted surface mass balances of debris-free glaciers observed between the southern and the inner parts of the Everest region (2007–15). Journal of Glaciology 63:637–651. DOI: 10.1017/jog.2017.30

Strickland, R. M., Covington, M. D., Gulley, J. D., Kayastha, R. B., and Blackstock, J. M.: Englacial Drainage Drives Positive Feedback Depression Growth on the Debris-Covered Ngozumpa Glacier, Nepal, Geophysical Research Letters, 50, e2023GL104389, https://doi.org/10.1029/2023GL104389, 2023.

Watson, C. S., Quincey, D. J., Smith, M. W., Carrivick, J. L., Rowan, A. V., and James, M. R.: Quantifying ice cliff evolution with multi-temporal point clouds on the debris-covered Khumbu Glacier, Nepal, J. Glaciol., 63, 823–837, https://doi.org/10.1017/jog.2017.47, 2017.

Wagnon, P., Lafaysse, M., Lejeune, Y., Maisincho, L., Rojas, M. and Chazarin, J.P., 2009. Understanding and modeling the physical processes that govern the melting of snow cover in a tropical mountain environment in Ecuador. Journal of Geophysical Research: Atmospheres 114(D19).

Table and caption

Table 1. Regional Climate Models (RCMs) chosen for this study and details of the Global Circulation Models (GCMs) from which these are derived. The NOAA RCM that was considered most representative of conditions in the Everest region. The temperature forcings used to project climate change beyond 2100 CE are global values and include no change in precipitation after 2100 CE.

CORDEX South Asia regional climate model	Driving CMIP5 global climate model	CMIP5 modelling centre	RCM name in this study	Future precipitation scenario	2100 CE mean temperature change from present day (°C)		2200 CE mean temperature change from 2100 CE (°C)		2300 CE mean temperature change from 2300 CE (°C)	
					RCP 4.5	RCP 8.5	RCP 4.5	RCP 8.5	RCP 4.5	RCP 8.5
ITTM-RegCM4	NOAA-GFDL-GFDL-ESM2M	National Oceanic and Atmospheric Administration (NOAA), USA	NOAA	Wet	1.4	3.8	0.5	2.8	0.7	4.1
IITM-RegCM4	CCCma-CanESM2	Canadian Centre for Climate Modelling and Analysis (CCCma), Canada	CCCma	Moderate	2.2	4.1	0.5	2.8	0.7	4.1
IITM-RegCM4	IPSL-CMSA-LR	Institue Pierre-Simon Laplace (IPSL), France	IPSL	Dry	1.6	3.8	0.5	2.8	0.7	4.1

Figures and captions

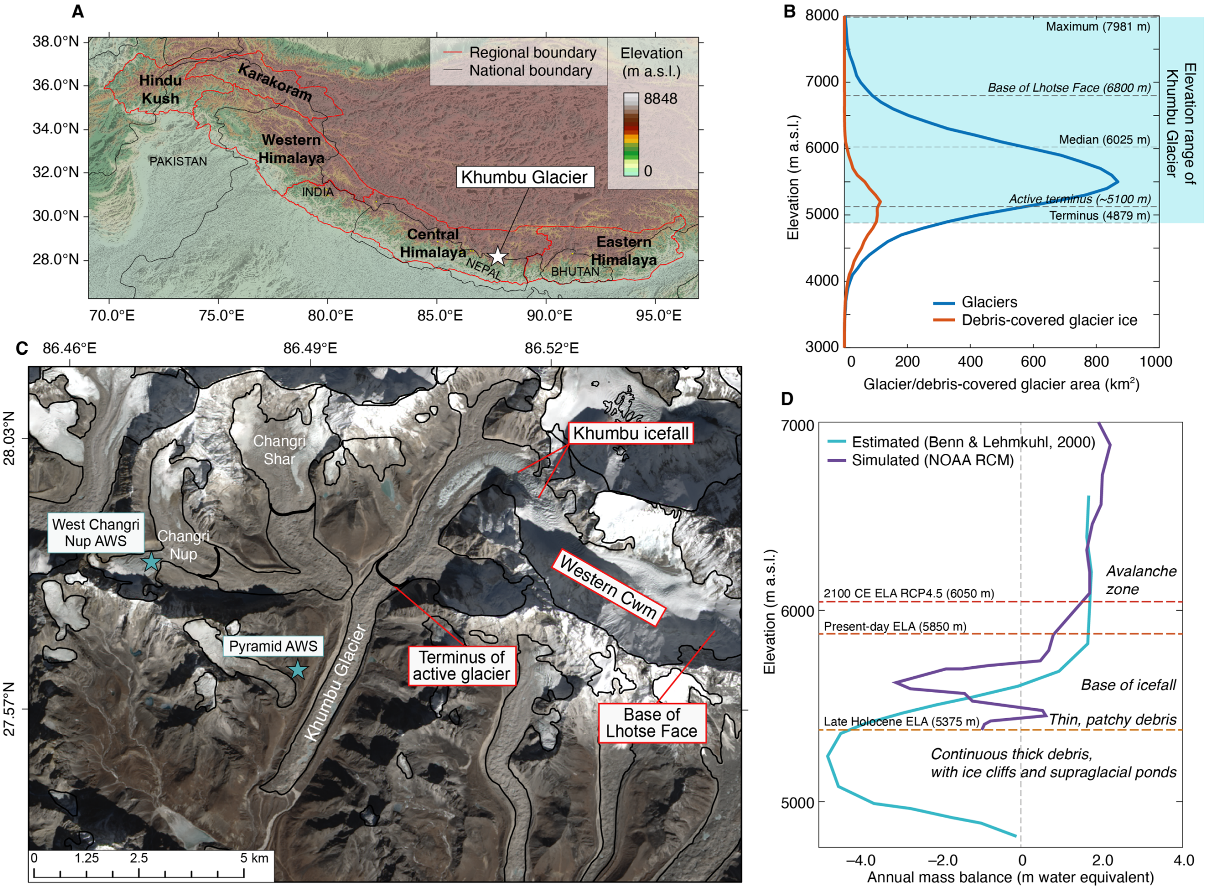

Figure 1: Khumbu Glacier location and context. (a) Location map of High Mountain Asia showing the location of the monsoon-influenced Central and Eastern Himalaya and Khumbu Glacier. (b) hypsometry of glaciers and debris-covered glacier ice in the Central and Eastern Himalaya compared with the elevations of Khumbu Glacier. (c) Satellite image of Khumbu Glacier showing the extent of supraglacial debris, location of the icefall, the extent of active ice flow inferred from observations of glacier velocity (black lines) and location of the automatic weather stations used for RCM downscaling (blue stars). (d) Estimated mass balance gradient for debris-covered glaciers in the Everest region (Benn and Lehmkuhl, 2000) compared with the glacier mass balance gradient simulated using the NOAA RCM and showing change in the equilibrium line altitude (ELA) of Khumbu Glacier in the historical and future simulations for the NOAA RCM RCP4.5 experiment.

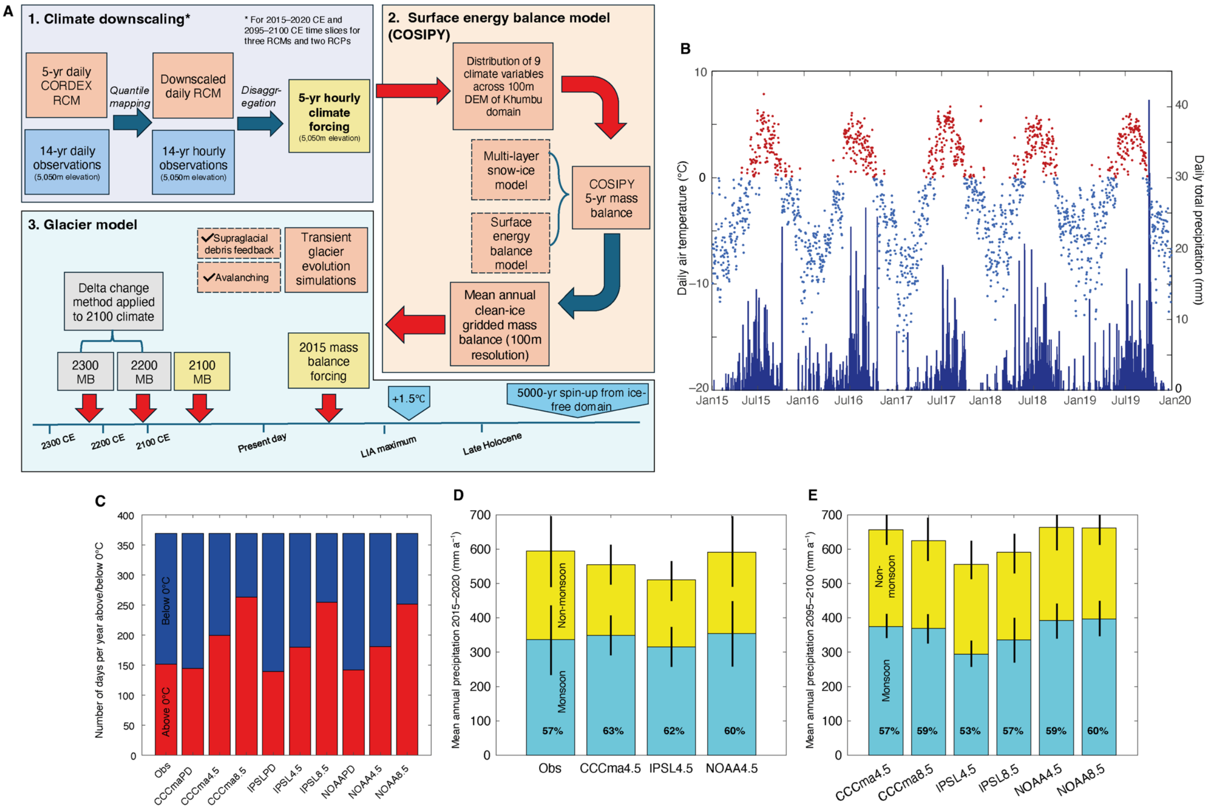

Figure 2: Climate-glacier model experimental design and evaluation of RCM downscaling. (a) Schematic diagram of the climate-glacier modelling approach showing the methods used for downscaling through quantile mapping and disaggregation of climate data. Note that this process does not apply to the post-2100 CE climate forcings which are subject to delta change. Surface energy balance modelling using COSIPY includes the pre-processing stage of meteorological distribution across the Khumbu domain, which is repeated for each RCM in the 2015–2020 CE climates and for the three RCMs and two RCPs for the 2095–2100 CE climates. The simulated mass balance is then used to force the glacier evolution model. (b) Daily mean temperature and daily total precipitation from the NOAA RCM for the present day (2015–2020 CE) following downscaling using quantile mapping with air temperature categorised into above freezing (red) and below freezing (blue). (c) Proportion of air temperatures above and below freezing for the present day for each RCM and RCP for the downscaled daily data compared with observations. (d) Annual precipitation totals for non-monsoon and monsoon with standard deviation between selected years shown by black bars for the downscaled daily data compared with observations. (e) Future (2095–2100 CE) time-slice annual precipitation totals for non-monsoon and monsoon months with standard deviation between selected years shown by black bars. In (d) and (e) the percentage of the total annual precipitation occurring during the monsoon is indicated by the value in bold text. (Obs = meteorological observations from AWS).

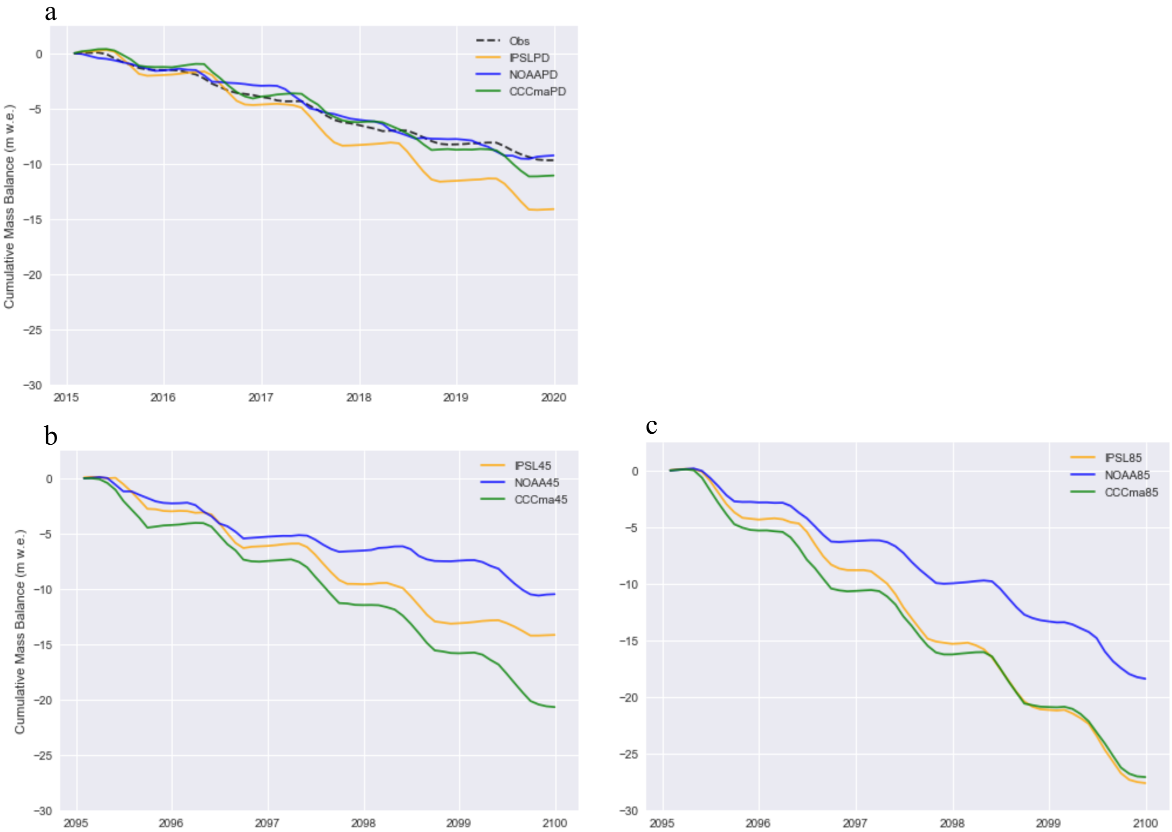

Figure 3: Spatially averaged cumulative clean-ice mass balance with clear seasonality for (a) the present day time-slice including the mass balance forced by the observations used for downscaling, and the end-of-century time-slice under (b) RCP4.5 and (c) RCP8.5. The low annual glacier-wide mass balance values shown here are the result of the extent of the model domain used to force the glacier model that includes the larger catchment beyond the glacier margins and therefore contains a higher proportion of lower elevations than those of the glacier itself. However the similar mass balance results for simulations forced by NOAA RCM and observations can be clearly seen (a), and the differences between the three RCMs is apparent in all time-slices (a-c).

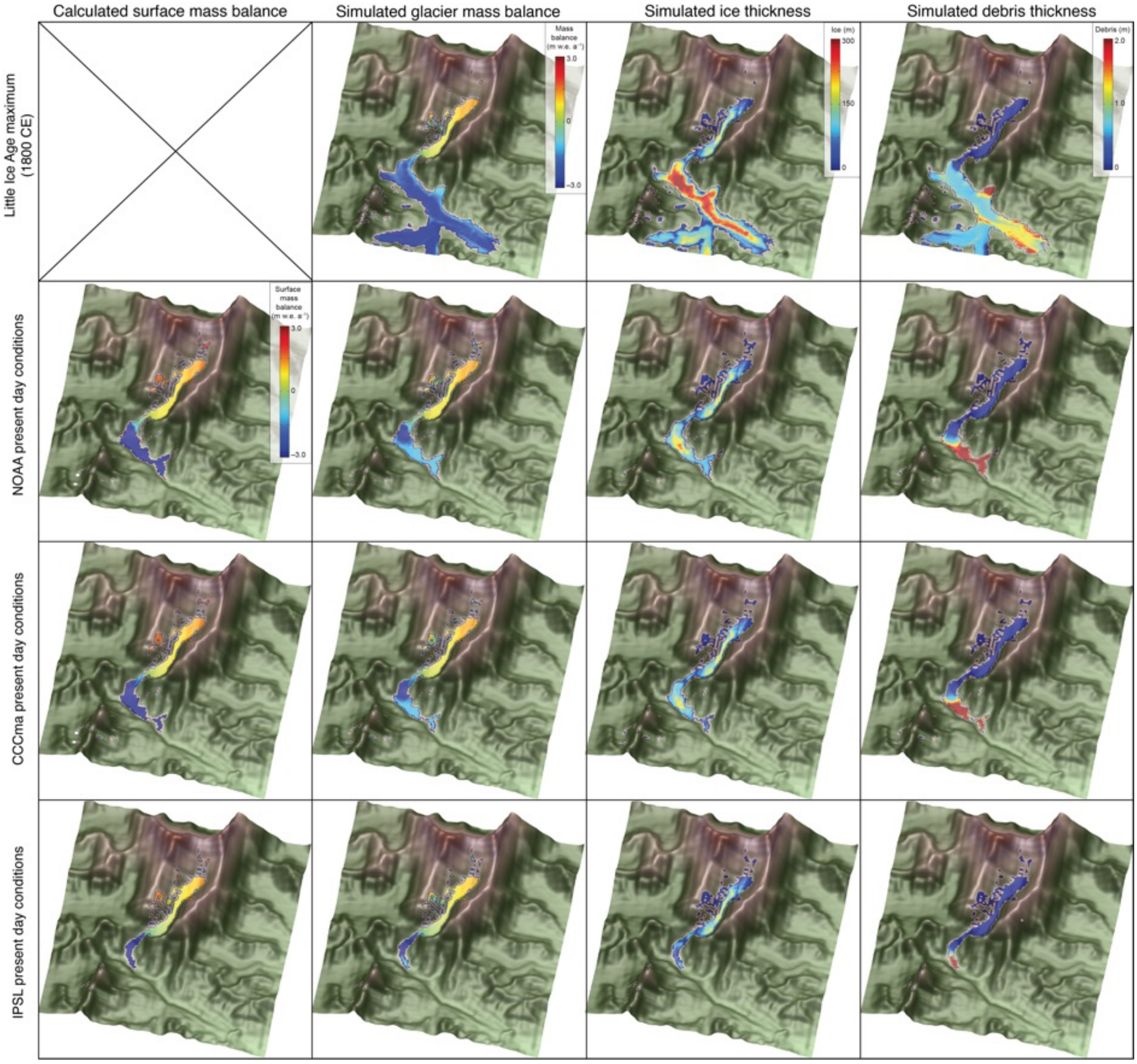

Figure 4. Glacier model sensitivity to surface energy and mass balance forcing, showing Little Ice Age (~1800 CE) glacier mass balance, ice thickness and debris thickness. Present-day results for surface mass balance calculated using each RCM with COSIPY showing glacier mass balance calculated using the same climate forcing following integration with the glacier model, simulated ice thickness, and simulated debris thickness.

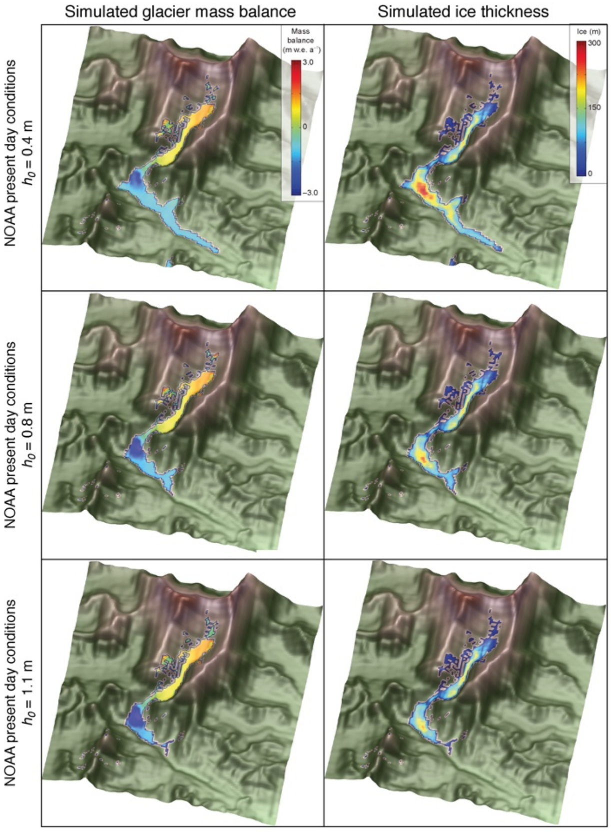

Figure 5. Glacier mass balance and ice thickness simulated using the NOAA RCM climate forcing and the resulting simulated ice thickness for h_0 values of 0.4 m, 0.8 m, and 1.1 m.

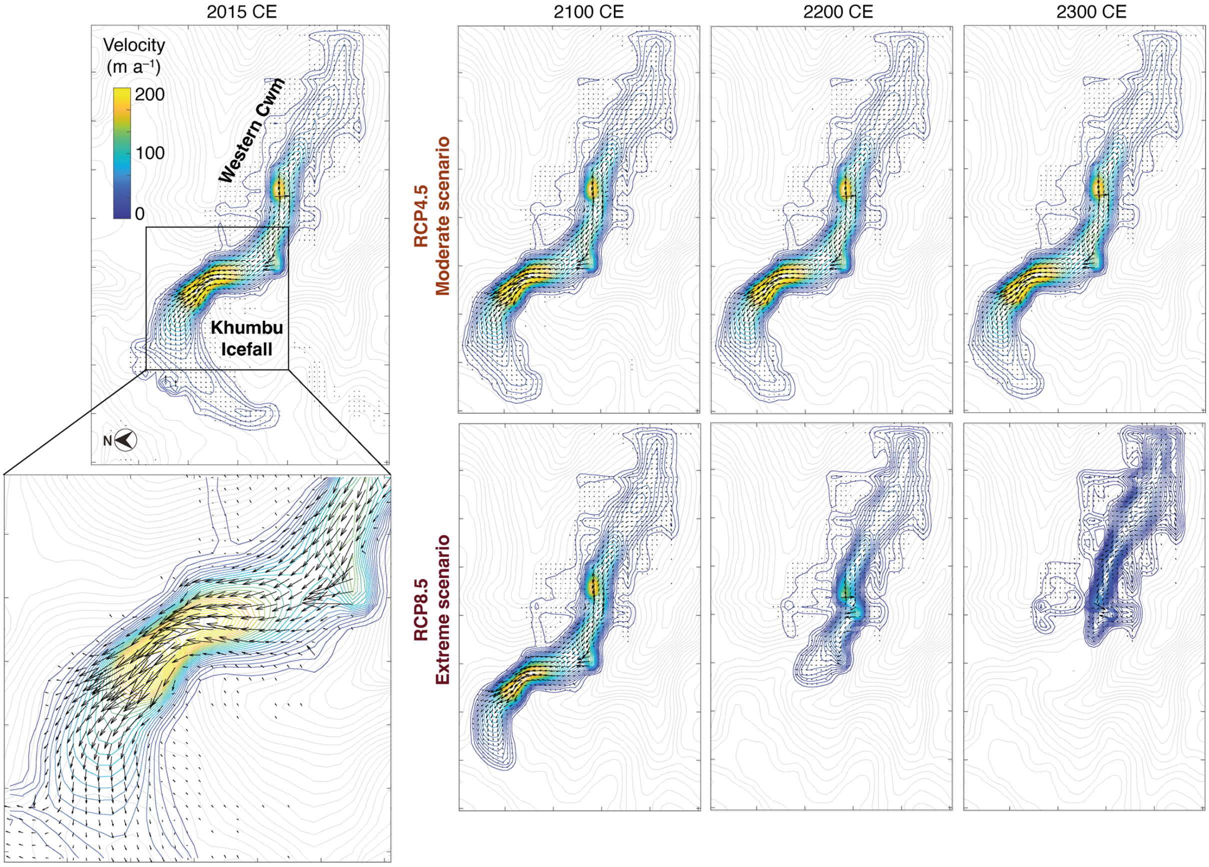

Figure 6. Simulated ice flow for Khumbu Glacier. Velocity-vector maps showing simulated ice flow magnitude and direction from the present day (2015–2020 CE) until 2300 CE under RCP4.5 and RCP8.5 using the downscaled NOAA climate forcing and a value for h_0 of 0.8 m. Simulated ice flow speed is shown as colour shading with blue contours, and the bed topography is shown by grey contours. The outermost contour in each plot represents the slowest ice flow close to the glacier margins with depth-integrated velocities of 5–10 m a^{-1}. Note that rapid flow across the Western Cwm indicated by one arrow shows the effects of avalanching rather than sustained glacier flow.

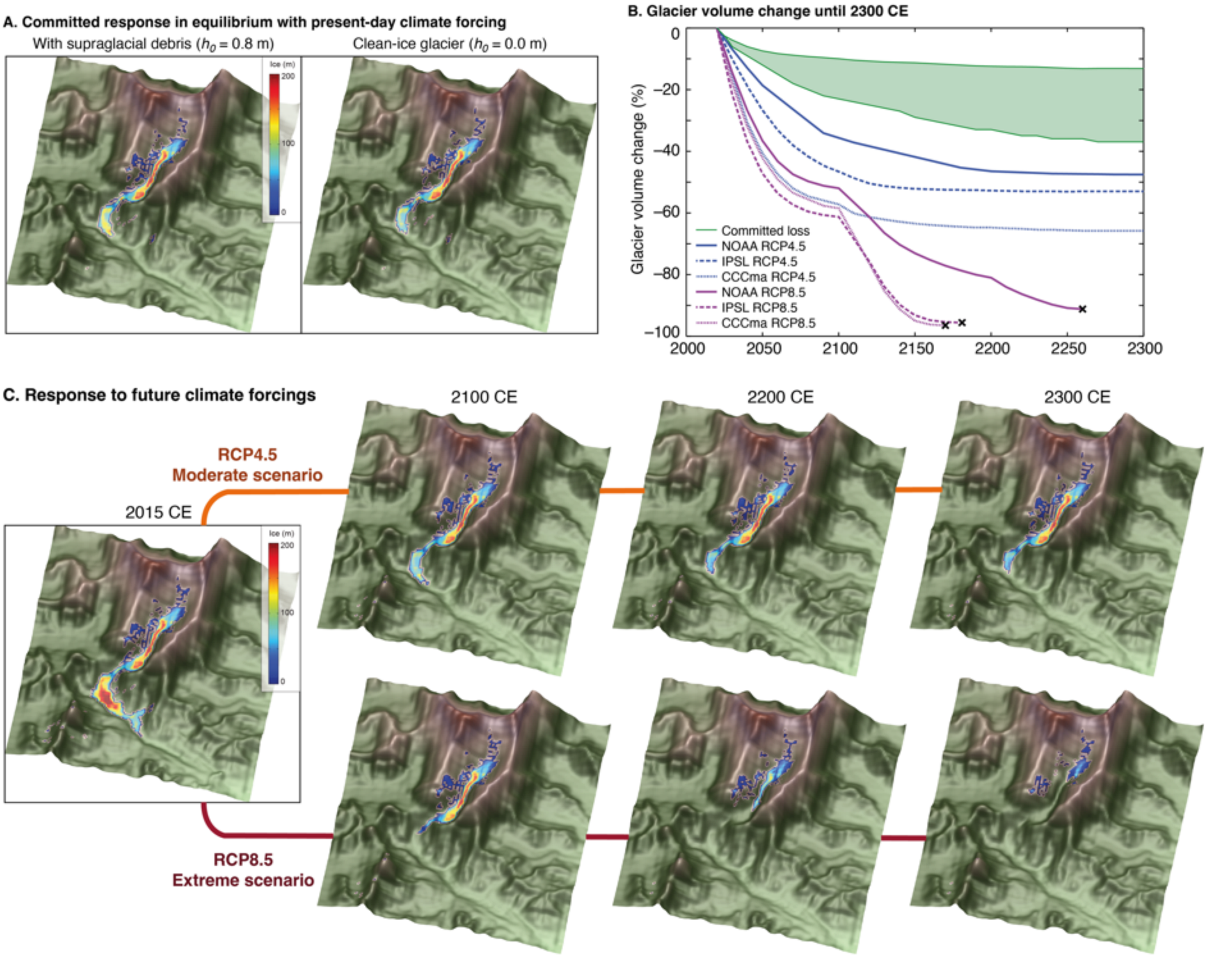

Figure 7. Future glacier volume change projections. (a) Equilibrium ice thickness accounting for the committed response to recent climate change using the downscaled NOAA RCM climate forcing with and without the effect of sub-debris melt. (b) Simulated glacier volume change from the present day (2015–2020 CE) until 2300 CE under RCP4.5 and RCP8.5 for the three downscaled RCMs. The black crosses mark when ice flow has declined sufficiently that the glacier is considered almost absent or no longer viable. The green shading shows the range of the committed volume loss due to historical warming. (c) Simulated ice thickness under RCP4.5 and RCP8.5 for 2100 CE, 2200 CE and 2300 CE using the downscaled NOAA RCM climate forcing.

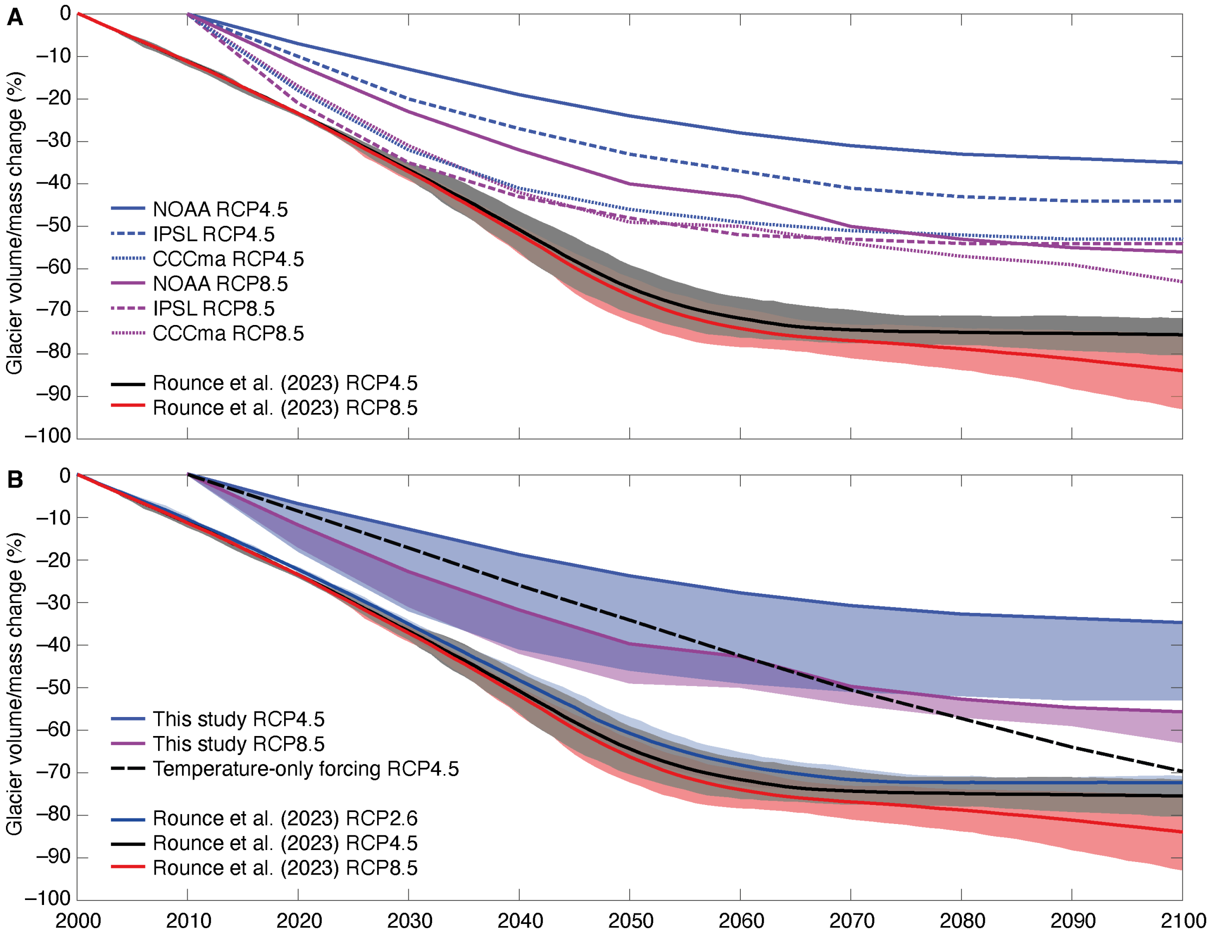

Figure 8. Comparison of projected shrinkage of Khumbu Glacier by 2100 CE from this study with those from Rounce et al. (2023) showing (a) results from each of the six experiments in this study with results from RCP4.5 and RCP8.5 from Rounce et al. (2023), and (b) comparison of results from this study where the bold line shows the NOAA RCM RCP4.5 and RCP8.5 experiments and the black dashed line shows the equivalent result for a simulation where precipitation does not change from the present-day value compared with results from Rounce et al. (2023) for RCP2.6, RCP4.5 and RCP8.5.

Appendix A

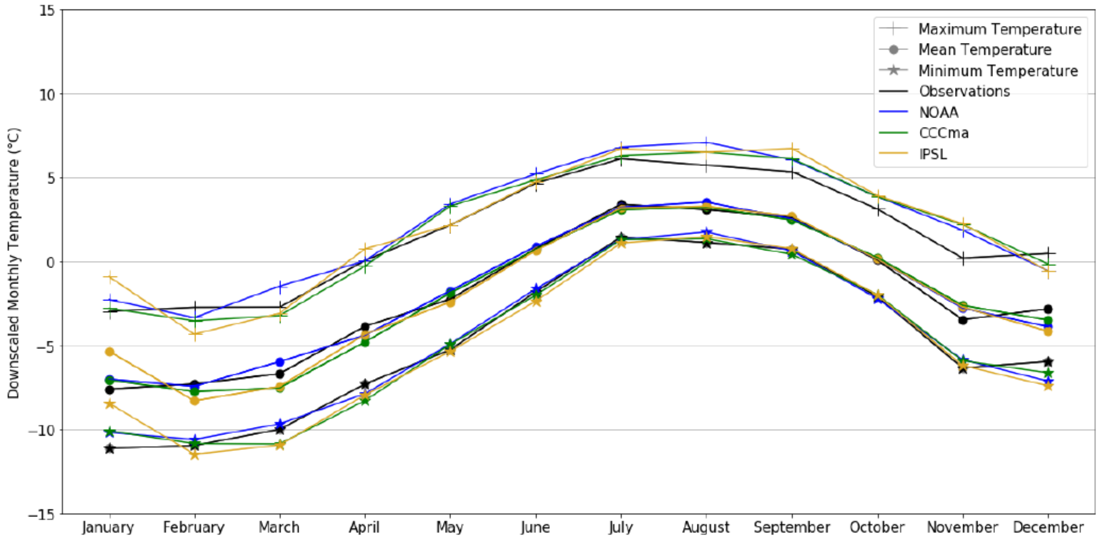

Figure A1: Downscaled monthly mean, maximum, and minimum temperature calculated for the present day time slice. Downscaled minimum and maximum temperatures were used to disaggregate to hourly temperatures following Debele et al. (2007). For the observations, minimum and maximum temperature are calculated from hourly data and then the monthly mean was calculated.

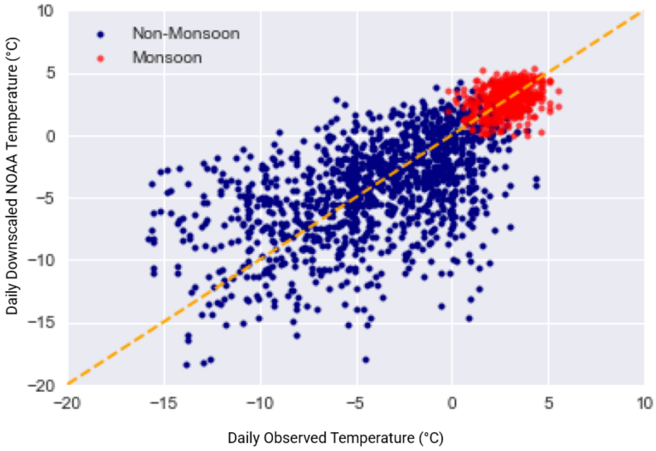

Figure A2: Daily downscaled temperature from the NOAA RCM against observations, split by monsoon/non-monsoon with a 1:1 line to aid analysis of the temperature distributions (dashed orange line).

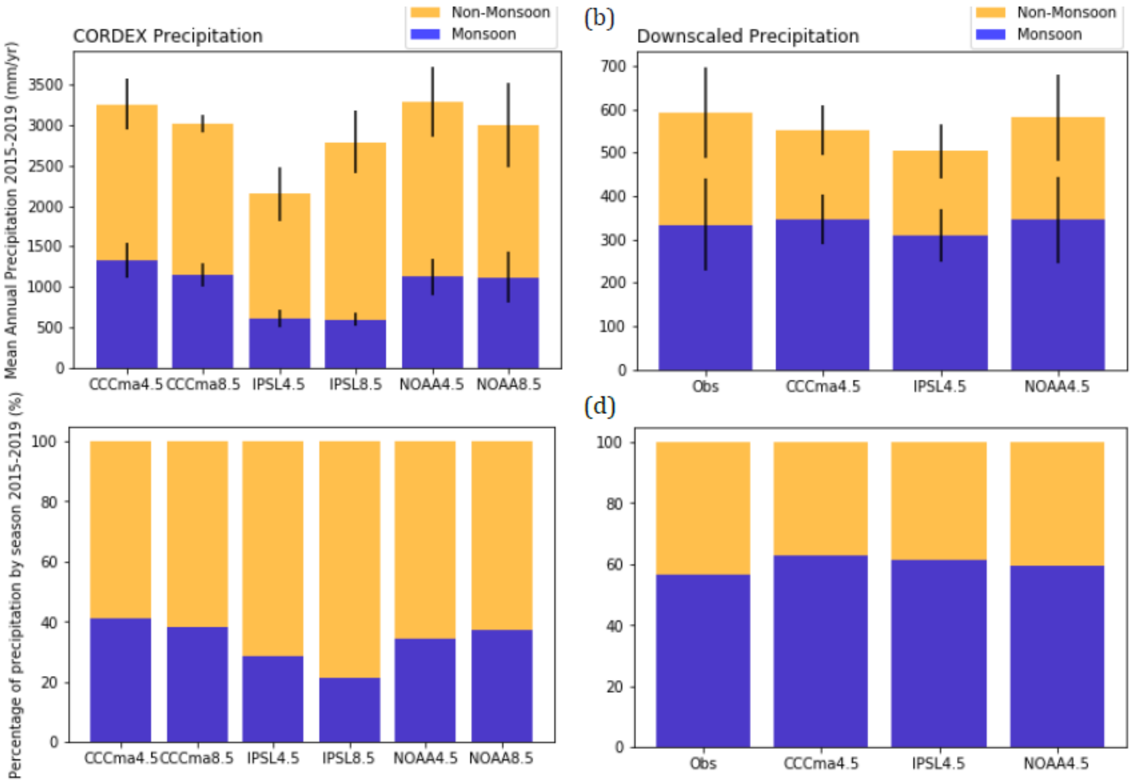

Figure A3. Annual precipitation totals for non-monsoon and monsoon months before and after downscaling with standard deviation between selected years shown by black bars (a and b) and as their seasonal percentages (c and d). Only the downscaled RCM outputs for RCP4.5 are used for the present day.